arXiv:1812.02550v2 [cond-mat.str-el] 10 Dec 2018

Ferromagnetic Mott State in Twisted Graphene Bilayers at the Magic Angle

Kangjun Seo[1], Valeri N. Kotov[2], and Bruno Uchoa[1*]
[1] *Department of Physics and Astronomy, University of Oklahoma, Norman, OK 73069, USA* and*
[2] *Department of Physics, University of Vermont, Burlington, VT 05405, USA*
(Dated: March 12, 2022)

We address the effective tight-binding Hamiltonian that describes the insulating Mott state of twisted graphene bilayers at a magic angle. In that configuration, twisted bilayers form a honeycomb superlattice of localized states, characterized by the appearance of flat bands with four-fold degeneracy. After calculating the maximally localized superlattice Wannier wavefunctions, we derive the effective spin model that describes the Mott state. We suggest that the system is an exotic *ferromagnetic* Mott insulator, with well defined experimental signatures.

Introduction.– Mott insulators describe materials that exhibit insulating behavior as a result of strong local interactions [1]. In those systems, strong on site repulsion penalizes the kinetic energy for electrons to hop between sites, rendering the electronic orbitals localized. The strong degree of localization of the electronic wavefunction favors antiferromagnetic alignment of the spins due to Pauli principle [2]. Recent experiments [3, 4] indicate that twisted graphene bilayers have a Mott state with an activation gap of $\Delta \approx 0.3$ meV that undergoes a metal-insulator transition in the vicinity of a superconducting phase [4, 5]. This system is purely made of carbon atoms, with additional degrees of freedom inherited from graphene [6]. That has motivated the question of whether the observed state could be described by a novel Mott insulator [7] or other exotic correlated states [8–12]. Unveiling the nature of the insulating state may be key to explain some of the the remarkable properties in the metallic phase.

By twisting two graphene sheets at a small angle of the order of $\theta \sim 1.1^\circ$, what was dubbed a "magic" angle, interference due to hopping between the layers leads to a Moire pattern and to a significant reconstruction of the mini bands in the Moire Brillouin zone, which become flat [13, 14]. Those flat bands have four-fold degeneracy, which is reminiscent of the valley and spin quantum numbers of the graphene sheets. In general, the confinement of interacting Dirac fermions in flat bands is expected to create an emergent SU(4) symmetry, as previously predicted in graphene heterostructures [15–17] and in graphene Landau levels [18–24]. Here, the Moire pattern forms a superlattice of quasi-localized states with the size of the unit cell set by the twist angle, as shown in Fig. 1.

In this Letter, we show that the low energy Hamiltonian of the flat bands at quarter filling maps into the *ferromagnetic* spin exchange Hamiltonian on a honeycomb superlattice,

$$\mathcal{H} = -\sum_{ij} J_{ij}\left(\frac{1}{2} + 2\tau_i^z\tau_j^z - 2\eta_{ij}\boldsymbol{\tau}_i^\perp\cdot\boldsymbol{\tau}_j^\perp\right)\left(\frac{1}{2} + 2\mathbf{S}_i\cdot\mathbf{S}_j\right), \tag{1}$$

where $\mathbf{S}_i$ is the localized spin on a superlattice site i, $\boldsymbol{\tau}_i = (\tau_i^x, \tau_i^y, \tau_i^z) \equiv (\boldsymbol{\tau}^\perp, \tau^z)$ is an orbital pseudospin operator that is reminiscent of the valley quantum numbers, and $J_{ij} > 0$ is the exchange coupling. The parameter $\eta_{ij} = -1$ when i, j belong to the same sublattice, in which case the exchange interaction has SU(4) symmetry, and $\eta_{ij} = 1$ otherwise, including nearest neighbor (NN) sites. This Hamiltonian acts in the Hilbert space which is spanned by four degenerate states per site, $|\alpha, \sigma\rangle$, with $\alpha = \pm$ and $\sigma = \uparrow, \downarrow$ for the two orbital pseudospins and spin quantum numbers respectively.

The existence of direct exchange ferromagnetism in an insulating state is uncommon [15] and reflects the very unusual shape of the Wannier orbitals in this system. Ferromagnetism has been recently observed in insulating van der Waals heterostructures of magnetic chromium trihalide materials, CrX_3 (X=I, Br, Cl) [25–27], which have crystalline field anisotropies that produce an ordered Ising state. To the best of our knowledge, we are not aware of any examples of ferromagnetic Mott states which do not involve orbital ordering via a superexchange mechanism [28, 29].

After performing calculations of the maximally localized Wannier orbitals of the Moire superstructure, we establish the parameters of a *minimal* interacting tight-

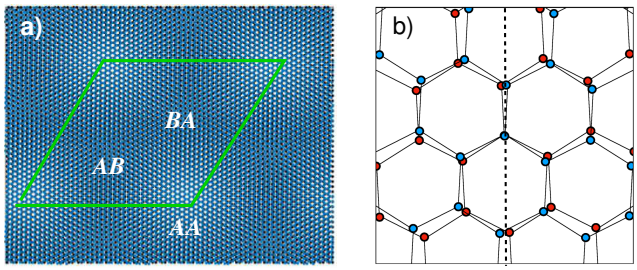


Figure 1: a) Moire pattern of twisted graphene bilayers for a twist angle of $\theta = 1.8^\circ$. Each layer has two sublattices, A and B. The pattern indicates regions of AA, AB, and BA alignment. Four-fold degenerate states are observed around the AA stacking regions. b) Twisted graphene bilayer rotated around A sites (AA region). At those points, the bilayer has D_3 symmetry, comprised of a C_3 rotation around the z axis and a C_2' rotation around the y axis (dashed line) in between two layers. Red and blue dots: top and bottom layer.

binding model that captures the Mott physics near the magic angle. We show that even though the orbitals are well localized in the Mott regime at quarter filling, surprisingly the direct *exchange* interaction between different sites is dominant and favors ferromagnetic spin order at zero temperature. While charging effects [30, 31], which were not taken into account, may change our conclusions, the scenario of zero temperature ferromagnetism in twisted graphene bilayers seems in line with the reduced degeneracy of the Landau levels measured with Shubnikov de Haas experiments near quarter filling [3]. We discuss the experimental signatures of this state.

Bloch Hamiltonian.– The free Hamiltonian for twisted graphene bilayers can be constructed at the lattice level using a parametrization for the hopping amplitudes between sites in the two different sheets,

$$\mathcal{H} = \begin{pmatrix} \mathcal{H}_g^{(1)} & \mathcal{H}_\perp \\ \mathcal{H}_\perp^\dagger & \mathcal{H}_g^{(2)} \end{pmatrix}, \tag{2}$$

where $\mathcal{H}_g$ is the graphene Hamiltonian and $\mathcal{H}_\perp$ is the interlayer hopping between the two sheets in real space. The Moire pattern can be used to construct Bloch states that are periodic in the superlattice vectors $\mathbf{T}_i$. For commensurate structures, the Moire lattice vectors are parametrized by two integers m and r, and correspond to the twist angle $\cos\theta = 1 - r^2/2(3m^2 + 3mr + r^2)$, or equivalently $\theta \approx r/\sqrt{3}m$ for small angles.

In a basis for Bloch states

$$\Phi_{\mathbf{k},\sigma} \equiv (|\varphi^{(1)}_{\mathbf{k},A,\sigma}\rangle, |\varphi^{(1)}_{\mathbf{k},B,\sigma}\rangle, |\varphi^{(2)}_{\mathbf{k},A,\sigma}\rangle, |\varphi^{(2)}_{\mathbf{k},B,\sigma}\rangle) \tag{3}$$

defined in the two sublattices A and B of each of the two layers $(1, 2)$, the Bloch Hamiltonian of the twisted system

$$\mathcal{H}_\mathbf{k}(\mathbf{r}, \mathbf{r}') = \sum_i \mathcal{H}(\mathbf{r}, \mathbf{r}' + \mathbf{T}_i) \mathrm{e}^{i\mathbf{k}\cdot\mathbf{T}_i} \tag{4}$$

satisfies $\mathcal{H}_\mathbf{k}(\mathbf{r}, \mathbf{r}' + \mathbf{T}_i) = \mathcal{H}_\mathbf{k}(\mathbf{r}, \mathbf{r}')e^{-i\mathbf{k}\cdot\mathbf{T}_i}$. In that basis,

$$[\mathcal{H}_\mathbf{k}]_{ab} = t^{ab}_\mathbf{k}(\mathbf{r}, \mathbf{r}') = \sum_j \mathrm{e}^{i\mathbf{k}\cdot\mathbf{T}_j} t^{ab}(\mathbf{r}, \mathbf{r}' + \mathbf{T}_j), \tag{5}$$

are the matrix elements of (2), with a, b indexes running over the four components of basis (3). The hopping amplitudes $t^{ab}(\mathbf{r}, \mathbf{r}') = \cos^2\theta_z V_\sigma(\mathbf{r} - \mathbf{r}') + \sin^2\theta V_\pi(\mathbf{r} - \mathbf{r}')$, where $\cos\theta_z = d/\sqrt{d^2 + (\mathbf{r} - \mathbf{r}')^2}$ with d the distance between the planes. $V_\sigma(\mathbf{r})$ and $V_\pi(\mathbf{r})$ are Slater-Koster functions [32], which decay exponentially and were parameterized following previous ab initio works [33, 34].

Diagonalization of the Bloch Hamiltonian results in a set of four-component Bloch eigenspinors $\hat{\psi}_{n,\mathbf{k}}(\mathbf{r}) \equiv \langle\mathbf{r}|\hat{\psi}_{n,\mathbf{k}}\rangle$ that satisfy $\hat{\psi}_{n,\mathbf{k}}(\mathbf{r} + \mathbf{T}) = \hat{\psi}_{n,\mathbf{k}}(\mathbf{r})\mathrm{e}^{i\mathbf{k}\cdot\mathbf{T}}$ and correspond to the energy spectrum $\varepsilon_n(\mathbf{k})$. We calculate the bands for a small twist angle of $\theta = 1.0845°$ ($m = 30$, $r = 1$) near the experimental magic angle $\theta_0 \sim 1.1°$.

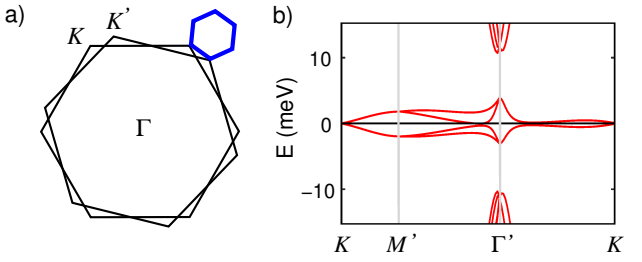


Figure 2: a) Moire Brillouin zone of the twisted graphene system (blue hexagon), containing the K and K' points at the corners. b) Flat bands in the Moire Brillouin zone for $\theta = 1.0845°$, near the magic angle $\theta_0 \sim 1.1°$. The Γ' point is at the center of the Moire Brillouin zone. M' is the mid point between K and K' points.

At that angle, the Bloch Hamiltonian is a $N_s \times N_s$ matrix with $N_s = 11164$ sites inside the Moire unit cell. The low energy bands ($n = 1, \ldots, 4$), shown in Fig. 2b, are four-fold degenerate at the K points (excluding the spin). They have a two-fold degeneracy at the other two high symmetry points of the Brillouin zone, Γ' and M', where they open up a gap between particle and hole branches. At the Γ' point, the Bloch states have C_3 and C'_{2y} symmetry, which involves at π rotation around the y axis placed half-way between the two layers (shown in Fig. 1b). We also find numerically that all Bloch eigenspinors satisfy the time reversal symmetry (TRS) relation $\mathcal{T}\hat{\psi}_{n,\mathbf{k}}(\mathbf{r}) = \hat{\psi}^*_{n,-\mathbf{k}}(\mathbf{r})$, with $\mathbf{k}$ measured from the center of the Moire Brillouin zone at Γ'. The K and K' points are hence related by TRS, and must have opposite π Berry phases. This fact indicates that the Bloch states of the twisted structure do not suffer from Wannier obstructions [35], and hence could be reconstructed through a proper basis of Wannier states.

Wannier orbitals.– From the Bloch states of the four low energy bands, one can extract the Wannier wave functions in the Moire unit cell,

$$|\mathbf{R}\nu\rangle = \frac{1}{N_s}\sum_\mathbf{k} \mathrm{e}^{-i\mathbf{k}\cdot\mathbf{R}} U_{n\nu}(\mathbf{k})|\hat{\psi}_{n,\mathbf{k}}\rangle, \tag{6}$$

where $\mathbf{R}$ is the center of the Wannier orbitals and $U_{n\nu}(\mathbf{k})$ some 4×4 unitary transformation. The four component Wannier spinors $\hat{W}_\nu(\mathbf{r} - \mathbf{R}) \equiv \langle\mathbf{r}|\mathbf{R}\nu\rangle$ are not unique since adding a phase to the Bloch state $\mathrm{e}^{-i\mathbf{k}\cdot\mathbf{r}}\hat{\psi}_{n\mathbf{k}}(\mathbf{r})$ corresponds to a new set of Wannier orbitals. We choose the set of maximally localized Wannier orbitals in finding the unitary transformation that minimizes their spread, $\Omega = \sum_\nu[\langle r^2\rangle_\nu - \langle r\rangle^2_\nu]$, with $\langle X\rangle_\nu \equiv \langle\mathbf{R}\nu|X|\mathbf{R}\nu\rangle$. The minimization was carried with the Wannier90 package [36]. The momentum space $\mathbf{k}$ mesh points are generated by the reciprocal supercell lattice vectors with 300×300 grid points using periodic boundary conditions, including all high symmetry points.

Following the symmetry arguments outlined in Ref. [37], we perform the minimization of the spread enforc-

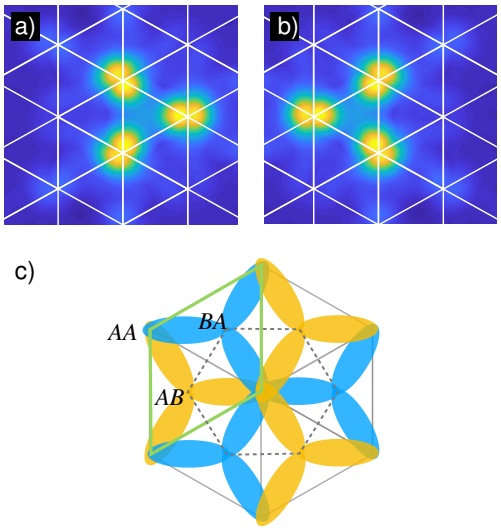


Figure 3: Wannier wavefunction in the Moire superlattice. Amplitude $|\hat{W}_+(\mathbf{r}-\mathbf{R}_j)| = |\hat{W}_-(\mathbf{r}-\mathbf{R}_j)|$ of the orbitals centered around (a) $j \in AB$ sites, and (b) $j \in BA$ sites, showing three sharp peaks. The orbitals $\hat{W}_\alpha$ have two-fold degeneracy per site, and are eigenstates of the C_3 rotation operator with eigenvalues ϵ ($\alpha = +$), and ϵ^* ($\alpha = -$). c) Sketch of the orbitals in the Moire unit cell (green line). Orange: AB centered Wannier orbitals. Blue: BA centered ones. The gray dotted line indicates the honeycomb superlattice formed by the center of the orbitals. Their unusual three peak structure indicates strong overlap between superlattice sites, favoring ferromagnetic ordering at zero temperature.

ing the C_3 and C'_{2y} symmetry for the Bloch states around the Γ' points. Those two symmetries describe a D_3 point symmetry group, which is a local symmetry of the lattice at AA site regions when the two graphene layers are rotated around a site [38], as depicted in Fig. 1b. In agreement with earlier results [37, 39], the Wannier functions that satisfy those symmetries have three sharp peaks centered around either the AB or BA sites, forming a honeycomb superlattice with two-fold degenerate orbitals per site, as shown in Fig. 3.

On a given Moire unit cell, we label the Wannier orbitals by the four-component spinors $\hat{W}_\nu = (w_{\nu,1}, w_{\nu,2}, w_{\nu,3}, w_{\nu,4})^T$. Among the four orbitals, $\hat{W}_\nu(r - \mathbf{R}_j)$, two are centered at $R_j \in AB$ sites and are eigenstates of the C_3 rotation operator, with eigenvalues $\epsilon = \mathrm{e}^{2\pi i/3}$ and ϵ^*. The other two are centered at $R_j \in BA$ sites and also have the same eigenvalues ϵ and ϵ^*. From now on, we will label the Wannier orbital spinors based on their C_3 rotation eigenvalues, $C_3\hat{W}_\alpha(\mathbf{r}-\mathbf{R}_j) = \mathrm{e}^{\alpha 2\pi i/3}\hat{W}_\alpha(\mathbf{r}-\mathbf{R}_j)$, with $\alpha = \pm$ and $R_j \in AB$ or BA. The two degenerate orbitals centered at a given superlattice site $\mathbf{R}_j$ are related by TRS, $\mathcal{T}\hat{W}_\alpha(\mathbf{r}-\mathbf{R}_j) = \hat{W}_{-\alpha}(\mathbf{r}-\mathbf{R}_j)$. Orbitals in NN superlattice sites $\mathbf{R}_i$ and $\mathbf{R}_j$ are related by the C'_2 rotation, $C'_2\hat{W}_\alpha(\mathbf{r}-\mathbf{R}_i) = \hat{W}_{-\alpha}(\mathbf{r}-\mathbf{R}_j)$.

Tight binding Hamiltonian.– The effective lattice model of this problem can be constructed by rewriting the Bloch Hamiltonian (4) into a kinetic energy term of the form

$$\mathcal{H} = \sum_{i,j} t_{\alpha\beta}(\mathbf{R}_{ij}) d^\dagger_{\alpha,\sigma}(\mathbf{R}_i) d_{\beta,\sigma}(\mathbf{R}_j), \tag{7}$$

where $\mathbf{R}_i$ indexes the sites of the honeycomb superlattice, $\mathbf{R}_{ij} \equiv \mathbf{R}_i - \mathbf{R}_j$ and the $d_\alpha(\mathbf{R})$ annihilates an electron with orbital of type α and spin σ at a given superlattice site. The hopping matrix elements between superlattice sites can be extracted from the matrix elements of Hamiltonian (2) in a basis of maximally localized Wannier functions,

$$t_{\alpha\beta}(\mathbf{R}_i) = \langle \mathbf{R}\alpha|\mathcal{H}|\mathbf{R}+\mathbf{R}_i, \beta\rangle. \tag{8}$$

Due to the translational invariance of the superlattice, $t_{\alpha\beta}(\mathbf{R}) = \langle 0, \alpha|\mathcal{H}|\mathbf{R}, \beta\rangle$. For NN sites, we find that $|t_{\alpha\alpha}|(1) \approx 0.384$ meV whereas for n-th NN sites $t_{\alpha,-\alpha}(n) = 0$. Hence, hopping between sites conserves the orbital pseudospin quantum number $\alpha = \pm$. $|t_{\alpha\alpha}|(n)$ has a non-trivial dependence with the distance between sites (see table I), in qualitative agreement with the findings of Ref. [37] for a significantly larger twist angle.

The Coulomb interactions between lattice sites can be written as $\mathcal{H}_C = \frac{1}{2}\int \mathrm{d}\mathbf{r}\mathrm{d}\mathbf{r}'\rho(\mathbf{r})\frac{e^2}{\kappa|\mathbf{r}-\mathbf{r}'|}\rho(\mathbf{r}')$, where $\rho(\mathbf{r})$ is the electron density and $\kappa \approx 5$ the dielectric constant of twisted bilayers encapsulated in boron nitride. We can rewrite this term in terms of $d_{\alpha,\sigma}$ operators by expressing the density $\rho(\mathbf{r}) = \sum_\sigma \hat{\Psi}^\dagger_\sigma(\mathbf{r})\hat{\Psi}_\alpha(\mathbf{r})$ in terms of field operators $\hat{\Psi}_\sigma(\mathbf{r}) = \sum_{\alpha,j}\hat{W}_\alpha(\mathbf{r}-\mathbf{R}_j)d_{\alpha,\sigma}$. The resulting Coulomb Hamiltonian has a direct term and also an exchange part, $\mathcal{H}_C = \mathcal{H}_d + \mathcal{H}_e$. The first term,

$$\mathcal{H}_d = \sum_{i,j} V_{\alpha\beta}(\mathbf{R}_{ij}) n_\alpha(\mathbf{R}_i) n_\beta(\mathbf{R}_j), \tag{9}$$

with $n_\alpha(\mathbf{R}) = \sum_\sigma d^\dagger_{\alpha,\sigma}(\mathbf{R}) d_{\alpha,\sigma}(\mathbf{R})$ the density operator and repeated α, β indexes to be summed. The Coulomb coupling is cast as an overlap integral of Wannier orbital spinors, $V_{\alpha\beta}(\mathbf{R}_{ij}) = \frac{1}{2}\int \mathrm{d}\mathbf{r}\mathrm{d}\mathbf{r}'|\hat{W}_\alpha(\mathbf{r}_i)|^2\frac{e^2}{\kappa|\mathbf{r}-\mathbf{r}'|}|\hat{W}_\beta(\mathbf{r}'_j)|^2$, with $\mathbf{R}_{ij} = \mathbf{R}_i - \mathbf{R}_j$ and $\mathbf{r}_j \equiv \mathbf{r} - \mathbf{R}_j$. The exchange part is

$$\mathcal{H}_e = \sum_{i\neq j} J_{\alpha\alpha',\beta\beta'}(\mathbf{R}_{ij})\, d^\dagger_{\alpha,\sigma}(\mathbf{R}_i) d^\dagger_{\beta,\sigma'}(\mathbf{R}_j) d_{\beta',\sigma'}(\mathbf{R}_i) d_{\alpha',\sigma}(\mathbf{R}_j), \tag{10}$$

where

$$J_{\alpha\alpha',\beta\beta'}(\mathbf{R}_{ij}) = \frac{1}{2}\int \mathrm{d}\mathbf{r}\mathrm{d}\mathbf{r}'\hat{W}^\dagger_\alpha(\mathbf{r}_i)\cdot\hat{W}_{\alpha'}(\mathbf{r}_j)\frac{e^2}{\kappa|\mathbf{r}-\mathbf{r}'|} \times \hat{W}^\dagger_\beta(\mathbf{r}'_j)\cdot\hat{W}_{\beta'}(\mathbf{r}'_i) \tag{11}$$

is the exchange coupling between lattice sites. In general, we find that the combinations $J_{\alpha\beta,\beta\alpha}(\mathbf{R}_{ij}) =$

(meV)	0	1	2	3	4	5	6
$\lvert t_{\alpha\alpha}\rvert$	0	0.384	0.005	0.447	0.162	0.084	0.007
$V_{\alpha\beta}$	21.2	16.9	16.7	15.6	12.6	11.58	9.68
$J_{\alpha\alpha}$	0	5.09	1.11	0.52	0.25	0.16	0.09
$J_{\alpha,-\alpha}$	0	−4.93	1.02	−0.51	−0.18	0.12	0.08

Table I: Electronic hopping amplitude $|t_{\alpha\alpha}|$, direct Coulomb interaction $V_{\alpha\beta}$ and exchange interaction $J_{\alpha\beta}$ for various nearest neighbor sites: on-site (0), and n-th nearest neighbors (n), with $n = 1 - 6$. Energies in meV calculated for $\kappa = 5$. $n = 1$, 3 and 4 correspond to sites in opposite sublattices. $J_{\alpha\alpha} \approx \pm J_{\alpha,-\alpha}$, with $+(-)$ for sites in the same (opposite) sublattice.

$J_{\alpha\beta,\alpha\beta}(\mathbf{R}_{ij}) = 0$ for $\alpha \neq \beta$, within the numerical precision. That includes the on site exchange (Hund's coupling), which is zero due to the orthogonality between same site Wannier spinors [15, 39]. From now on, we define the *only* non-zero combination $J_{\alpha\alpha,\beta\beta} \equiv J_{\alpha\beta}$.

The numerical values of the hopping energy, Coulomb interaction and the exchange interaction for n-th NNs, is shown in table I, which is the first main result of the paper. We find the on-site Hubbard $U_{\alpha\beta} \equiv V_{\alpha\beta}(0) = 21.2$ meV, which is much larger than the first NN hopping $t(1)$, and hence the ratio $U/t(1) \sim 55$ falls comfortably in the realm of the Mott regime.

The exchange interaction for first NN sites ($n = 1$) is $|J_{\alpha\beta}(1)| \approx 5$ meV. In general, the diagonal terms $J_{\alpha\alpha}(n) > 0$ are positive definite, whereas the off diagonal ones can be either positive or negative, $J_{\alpha,-\alpha}(n) \approx \pm J_{\alpha\alpha}(n)$, with $+$ $(-)$ for i, j sites in the same (opposite) sublattice, as shown in table I. For sites in the same sublattice, the fact that $J_{\alpha\beta}(n) \approx J_{\alpha\alpha}(n) > 0$ is the same for all four combinations of $\alpha, \beta = \pm$ indexes hints at an emergent SU(4) symmetry between spin and orbital degrees of freedom at quarter filling. For sites in opposite sublattices, the exchange interaction has SU(2) symmetry in the spin. It has also both ferro ($J_{\alpha\alpha} > 0$) and antiferromagnetic ($J_{\alpha,-\alpha} < 0$) correlations in the orbital sector, depending on the orientation of the pseudospins.

Since Hund's coupling is zero, at quarter filling the lower flat bands are in the unitary limit [40], with each Moire superlattice site $\mathbf{R}_j$ being singly occupied and having a well defined spin σ and orbital quantum number $\alpha = \pm$. Mapping the exchange term in terms of spin $\mathbf{S}_i = \frac{1}{2} d^\dagger_{\alpha,\sigma}(\mathbf{R}_i)\vec{\sigma}_{\sigma\sigma'} d_{\alpha,\sigma'}(\mathbf{R}_i)$ and pseudospin $\boldsymbol{\tau}_i = \frac{1}{2} d^\dagger_{\alpha,\sigma}(\mathbf{R}_i)\vec{\sigma}_{\alpha\beta} d_{\beta,\sigma}(\mathbf{R}_i)$ operators, the result is the ferromagnetic exchange interaction announced in Eq. (1), with $J_{ij} \equiv J_{\alpha\alpha}(n) > 0$ [41]. This Hamiltonian favors ferromagnetic alignment of the spins at zero temperature ($T = 0$). In the orbital sector different states are possible, including canted magnetism with ferromagnetic order in the pseudospin τ^z component, accompanied by staggered (antiferromagnetic) order in the transverse, $\boldsymbol{\tau}^\perp$ direction.

The superexchange interaction follows from second order perturbation theory in the hopping energy [42, 43] and has the same form as the exchange term in Eq. (1) for $\eta_{ij} = -1$ [15]. The superexchange term has SU(4) symmetry and favors antiferromagnetic alignment between nearest neighbor sites due to Pauli principle. It's coupling $J \to -t^2/U \approx -0.01$ meV is very small compared to the exchange one, and can be safely igonored.

Ferromagnetic Mott state.– Mott-Hubbard insulators have strongly localized states and are known to be overwhelmingly antiferromagnetic due to strong superexchange interactions ($t^2/U \gg J$) [44–46]. Ferromagnetism occurs mostly either in metallic systems or in metallic bands hybridized with localized moments via the Anderson impurity mechanism [44, 45, 47]. Within the Hubbard model framework, the only credible mechanism for spin ferromagnetism exists for multi-orbital systems in the context of the Kugel-Khomskii model [42, 46], where superexchange can become effectively ferromagnetic in the presence of staggered orbital ordering.

We conjecture that the flat bands in twisted graphene bilayers are in a way intermediate between ferromagnetic bad metals and antiferromagnetic Mott-Hubbard insulators. Due to the exotic shape of the Wannier orbitals, the hierarchy between hopping, direct exchange and the local Hubbard interaction, $t \ll J \ll U$, leads to an anomalously small superexchange. In the charge sector the Mott gap is also anomalously small, $\Delta \sim 0.3$ meV $\ll W \ll U$, where $W \sim 5$ meV is the bandwidth, and the system undergoes an insulator-metal transition at $T \approx 4$K [3].

In spite of the fact that U/t is large, the strong overlap between the orbitals found in the non-interacting theory suggests that the system is potentially close to an insulator-metal transition [1] due to a charge fluctuation mechanism which presently is not well-understood [30, 31]. Nevertheless, the effective spin model we propose in this work should not depend on the details of this mechanism, as long as the system remains quarter filled and does not undergo a charge-ordering transition (potentially accompanied by dimerization) due to Coulomb interactions. In carbon lattices, which are notoriously stiff [48], charge density wave instabilities are hindered by the high elastic energy cost for the system to deform

the lattice and restore charge neutrality.

Experimental signatures.– Since the honeycomb superlattice is not frustrated, it will exhibit ferromagnetic spin order at $T = 0$ in the universality class of the ferromagnetic (spin S) Heisenberg model. It is well known that the magnetization M, correlation length ξ and the spin susceptibility χ exhibit peculiar features in two dimensions, since for any $T \neq 0$ the system is disordered, with zero Curie temperature. The model has been extensively studied both in zero and finite external magnetic field H on various lattices [49–52]. At finite field $H \neq 0$, $M(H)$ is finite and strongly temperature dependent. In the regime $T/J \ll 1$, which can take place for $T \approx 2$K (where $T/J \approx 1/25$), a weak magnetic field of $H \approx 0.2$T (i.e. $H/J \approx 1/250$) already provides nearly maximum magnetization [50, 51]. The susceptibility $\chi(H)$ is zero for $T = 0$ and $H \neq 0$ and exhibits a characteristic finite-temperature peak at $T = T_\chi$ which scales in a well-defined way with external field.

It has been established experimentally that doping away from the Mott insulating phase leads to metallic (and even superconducting) behavior [3, 4]. Therefore the structure of the ground state and excitation spectrum of this unconventional metallic state is of great experimental and theoretical interest. A profound new feature has emerged at finite magnetic field, which persists both in weak (Shubnikov-de Haas oscillations) and strong field limits (Quantum Hall effect), for hole doping [3, 4]. Those measurements suggest a small Fermi surface that develops from doping the correlated insulating phase, accompanied by a possible symmetry breaking of yet unknown origin. The resulting state has a fermionic degeneracy of 2, indicating a reduction of the original four-fold band degeneracy by a factor of 2.

This behavior is consistent with the system being in the proximity to a ferromagnetic Mott state, in which the spins align when nudged by an infinitesimally weak field. At the same time, any long-range order in the orbital sector is expected to be much more fragile and disappear quickly due to charge disorder and motion of holes in the metallic state. Therefore we conjecture that in the weak field limit, the ground state emerging from doping the ferromagnetic insulator would be a ferromagnetic, spin-polarized, strongly-correlated metal, with the orbital pseudospin symmetry preserved.

Conclusions.– We have derived the effective spin model that describes the Mott phase of twisted graphene bilayers at the magic angle. After calculating the maximally localized Wannier wavefunctions from the lattice, we propose that the system forms a novel *ferromagnetic* Mott state at quarter filling, with clear experimental signatures.

Acknowledgements.– BU Acknowledges P. Jarillo-Harillo, T. Senthil, and K. Beach for discussions. K.S. and B. U. acknowledge NSF CAREER grant No. DMR-1352604 for support.

Note added.– After the submission of this work, we became aware of Ref. [53], which also found a ferromagnetic ground state using different arguments. We thank O. Vafek for pointing it out.

* Electronic address: uchoa@ou.edu

[1] M. Imada, A. Fujimori, and Y. Tokura, Rev. Mod. Phys. **70**, 1039 (1998).
[2] A. Auerbach, Interacting Electrons and Quantum Magnetism, (Springer-Verlag, 1998).
[3] Y. Cao, V. Fatemi, S. Fang, K. Watanabe, T. Taniguchi, E. Kaxiras, and P. Jarillo-Herrero, Nature **556**, 80 (2018).
[4] Y. Cao, V. Fatemi, S. Fang, K. Watanabe, T. Taniguchi, E. Kaxiras, and P. Jarillo-Herrero, Nature **556**, 43 (2018).
[5] Matthew Yankowitz, Shaowen Chen, Hryhoriy Polshyn, K. Watanabe, T. Taniguchi, David Graf, Andrea F. Young, and Cory R. Dean, arXiv:1808.07865 (2018).
[6] A. H. Castro Neto, N. M. R. Peres, F. Guinea, A. Geim, K. Novoselov, Rev. Mod. Phys. **81**, 109 (2018).
[7] Hoi Chun Po, Liujun Zou, Ashvin Vishwanath, and T. Senthil, Phys. Rev. X **8**, 031089 (2018).
[8] Bikash Padhi, Chandan Setty, and Philip W. Phillips, Nano Lett. **18**, 6175 (2018).
[9] X. Y. Xu, K. Law, P. A. Lee, Phys. Rev. B **98**, 121406(R) (2018).
[10] V. Y. Irkhin, Y. N. Skryabin, JETP Lett. **107**, 651 (2018).
[11] A. Thomson, S. Chatterjee, S. Sachdev, M. S. Scheurer, Phys. Rev. B: Condens. Matter Mater. Phys. **98**, 075109 (2018).
[12] J. F. Dodaro, S. A. Kivelson, Y. Schattner, X. -Q. Sun, C. Wang, Phys. Rev. B: Condens. Matter Mater. Phys. **98**, 075154 (2018).
[13] J. M. B. Lopes dos Santos, N. M. R. Peres, and A. H. Castro Neto, Phys. Rev. Lett. **99**, 256802 (2007).
[14] R. and A. H. MacDonald, Proc. Nat. Acad. Sci. **108**, 12233 (2011).
[15] B. Uchoa, V. N. Kotov and M. Kindermann, Phys. Rev. B **91**, 121412(R) (2015).
[16] X. Dou, V. N. Kotov and B. Uchoa, Sci. Rep. **6** (2016).
[17] Cenke Xu, and Leon Balents, Phys. Rev. Lett. **121** 087001 (2018).
[18] M. O. Goerbig, Rev. Mod. Phys. **83**, 1193 (2011).
[19] A. F. Young *et. al.,* Nature Phys. **8**, 550 (2012).
[20] A. F. Young, et al., Nature **505**, 528 (2013).
[21] K. Nomura and A. H. McDonald, Phys. Rev. Lett. **96**, 256602 (2006).
[22] J. Alicea and M. P. A. Fisher, Phys. Rev. B **74**, 075422 (2006).
[23] D. A. Abanin, B. E. Feldman, A. Yacoby and B. I. Halperin, Phys. Rev. B **88**, 115407 (2013).
[24] I. Sodemann, and A. H. MacDonald, Phys. Rev. Lett. **112**, 126804 (2014).
[25] B. Huang *et al.*, Nature **546**, 7657 (2017), pp. 270--273.
[26] W. B. Yelon and R. Silberglitt, Phys. Rev. B **4**, 2280 (1971).
[27] E. J. Samuelsen, R. Silberglitt, G. Shirane, and J. P. Remeika, Phys. Rev. B **3**, 157 (1971).

[28] A. S. Erickson, S. Misra, G. J. Miller, R. R. Gupta, Z. Schlesinger, W. A. Harrison, J. M. Kim, and I. R. Fisher, Phys. Rev. Lett. **99**, 016404 (2007).

[29] K. I . Kugel, and D. Khomskii, Sov. Phys. JETP **37**, 725 (1973).

[30] J.M. Pizarro, M.J. Calderon, and E. Bascones, arXiv:1805.07303 (2018).

[31] F. Guinea, N. R. Walet, arXiv:1806.05990 (2018).

[32] The functions $V_\sigma(\mathbf{r}) = V^0_{pp\sigma}\exp[-(|\mathbf{r}|-d)/\lambda]$ and $V^0_\pi(\mathbf{r}) = V^0_{pp\pi}\exp[-(|\mathbf{r}|-a/\sqrt{3})/\lambda]$, with $d = 3.35$Å the interlayer distance, $a = 2.42$Å in in-plane lattice constant, $V^0_{pp\sigma} = 0.39$eV, $V^0_{pp\pi} = -3.09$eV and $\lambda = 0.27$Å. See Ref. [33].

[33] X. Lin, and D. Tománek, Phys. Rev. B **98**, 081410(R) (2018).

[34] M. S. Tang, C. Z. Wang, C. T. Chan, and K. M. Ho, Phys. Rev. B **53**, 979, (1996).

[35] H. C. Po, H. Watanabe, and A. Vishwanath, Phys. Rev. Lett. **121**, 126402 (2018).

[36] A. A. Mostofi, J. R. Yates, G. Pizzi, Y.-S. Lee, I. Souza, D. Vanderbilt, and N. Marzari, Comput. Phys. Commun. 185, 2309 (2014).

[37] J. Kang, and O. Vafek, Phys. Rev. X **8**, 031088 (2018).

[38] Noah F. Q. Yuan and Liang Fu, Phys. Rev. B 98, 045103 (2018).

[39] M. Koshino, N. F. Q. Yuan, T. Koretsune, M. Ochi, K. Kuroki, and L. Fu, Phys. Rev. X **8**, 031087 (2018)

[40] B. Coqblin, and A. Blandin, Adv. in Phys., 17:67, 281 (1968).

[41] For details, see supplementary materials.

[42] K. I. Kugel and D. I. Khomskii, Sov. Phys. Uspekhi **25**, 231 (1982).

[43] J. W. F. Venderbos, R. M. Fernandes, arXiv:1808.10416 (2018).

[44] Philip W. Anderson, "Theory of Magnetic Exchange Interactions: Exchange in Insulators and Semiconductors (in Solid State Physics, edited by F. Seitz and D. Turnbull, vol. 14)," (Academic Press, 1963) pp. 99 – 214.

[45] P. W. Anderson, Phys. Rev. **115**, 2 (1959).

[46] Daniel I. Khomskii, Basic Aspects of the Quantum Theory of Solids (Cambridge University Press, 2010).

[47] T. Moriya, Spin Fluctuations in Itinerant Electron Magnetism (Springer-Verlag, 1985).

[48] Jae-Ung Lee, Duhee Yoon, and Hyeonsik Cheong, Nano Lett. **12**, 4444 (2012).

[49] Peter Kopietz and Sudip Chakravarty, Phys. Rev. B **40**, 4858–4870 (1989).

[50] T. N. Antsygina, M. I. Poltavskaya, I. I. Poltavsky, and K. A. Chishko, Phys. Rev. B **77**, 024407 (2008).

[51] I. Juhasz Junger, D. Ihle, L. Bogacz, and W. Janke, Phys. Rev. B **77**, 174411 (2008).

[52] At low $T \ll J$, the zero-field susceptibility exhibits characteristic 2D deviation from the conventional Curie-Weiss law, $T\chi \sim (T/J)^3 \exp(2cJ/T)$, while the magnetization is zero at any finite T.

[53] Jian Kang, Oskar Vafek, arXiv:1810.08642 (2018).

Supplementary Materials of "Ferromagnetic Mott state in twisted graphene bilayers at the magic angle"

Kangjun Seo, Valeri N. Kotov and Bruno Uchoa
Department of Physics and astronomy, University of Oklahoma, Norman, OK 73019, USA and
Department of Physics, University of Vermont, Burlington, VT 05405, USA

MOIRÉ SUPERLATTICE

Each graphene layer consists of two sublattices (A_1, B_1 in layer 1 and A_2, B_2 in layer 2). The positions of the carbon atoms in each sublattice in layer 1 (bottom layer) are

$$\mathbf{r}_{B_1} = n\,\mathbf{a}_1 + m\,\mathbf{a}_2, \quad \mathbf{r}_{A_1} = \mathbf{r}_{B_1} + \boldsymbol{\delta}_1, \tag{1}$$

where n and m are integers, $\boldsymbol{\delta}_1 = 2/3(\mathbf{a}_1 + \mathbf{a}_2)$, and $\mathbf{a}_j$ are basis vectors of the unit cell ,

$$\mathbf{a}_1 = a\,(1,0), \quad \mathbf{a}_2 = a\,(1,\sqrt{3})/2 \tag{2}$$

with the lattice parameter a =2.46 Å. When the layers are not twisted ($\theta = 0$), the horizontal position of site B_2 is the same as of site B_1:

$$\mathbf{r}_{B_2} = n\,\mathbf{a}_1 + m\,\mathbf{a}_2, \quad \mathbf{r}_{A_2} = \mathbf{r}_{B_2} + \boldsymbol{\delta}_1, \tag{3}$$

After the rotation, the lattice vectors of layer l are given by

$$\mathbf{a}_i(l) = R(\pm\theta/2)\,\mathbf{a}_i(l), \quad R(\theta) = \begin{pmatrix} \cos\theta & \sin\theta \\ -\sin\theta & \cos\theta \end{pmatrix} \tag{4}$$

with $R(\theta)$ being the rotation matrix around B_1 and B_2. Then the reciprocal lattice vectors becomes

$$\mathbf{b}_i(l) = R(\pm\theta/2)\,\mathbf{b}_i, \tag{5}$$

where $\mathbf{b}_1 = \frac{2\pi}{a}\,(1,-1/\sqrt{3})$ and $\mathbf{b}_2 = \frac{2\pi}{a}\,(0,2/\sqrt{3})$.

The lattice is commensurate if [1, 3–5]

$$\cos\theta = \frac{3m_0^2 + 3m_0 r + r^2/2}{3m_0^2 + 3m_0 r + r^2}, \tag{6}$$

where m_0 and r are coprime positive integers. The superlattice vectors $\mathbf{T}_{1,2}$ can be expressed in terms of m_0, r, and $\mathbf{a}_{1,2}$. These expressions are different when r is either divisible or nondivisible by 3. The number of sites in each supercell is

$$N(m_0, r) = \begin{cases} 4(3m_0^2 + 3m_0 r + r^2), & r \neq 3n, \\ 4(3m_0^2 + 3m_0 r + r^2)/3, & r = 3n. \end{cases} \tag{7}$$

The linear size of the superlattice cell is

$$|\mathbf{T}_1| = |\mathbf{T}_2| = a\sqrt{N}/2. \tag{8}$$

The Moiré period L is related to the twist angle,

$$L = \frac{a}{2\sin(\theta/2)}. \tag{9}$$

In our numerical calculations, we use $m_0 = 30$ and $r = 1$ which correspond to $\theta = 1.0849°$, $L = 129.9196$ Å, and $N = 11164$. The superlattice vectors and the corresponding reciprocal superlattice vectors are

$$\mathbf{T}_1 = L\,(0,-1), \quad \mathbf{T}_2 = L\,(\sqrt{3}/2,-1/2). \tag{10}$$

$$\mathbf{G}_1 = \frac{2\pi}{L}\,(-1/2, -\sqrt{3}/2), \quad \mathbf{G}_2 = \frac{2\pi}{L}\,(1, 0). \tag{11}$$

The two nonequivalent Dirac points are

$$\mathbf{K}_1 = \frac{\mathbf{G}_1 + 2\mathbf{G}_2}{3}, \quad \mathbf{K}_2 = \frac{2\mathbf{G}_1 + \mathbf{G}_2}{3}. \tag{12}$$

The existence of a commensuration depends only on the relative rotation of the lattice vectors of each layer, and not on the structure of the unit cells of each layer. These amount to different choices of initial basis vectors within each cell. [2]

MICROSCOPIC HAMILTONIAN OF GRAPHENE BILAYER

It is convenient to enumerate the sites in the sublattice in each layer using two integer valued vectors $\mathbf{j} = (i, j)$ and $\mathbf{x} = (n, m)$, where $\mathbf{j}$ labels the positions of the supercell and $\mathbf{x}$ enumerates the sites in the supercell. Then, the Hamiltonian has the form

$$\begin{aligned}\mathcal{H} \;=\; & \sum_{\langle \mathbf{ix},\mathbf{jy}\rangle, l=1,2,\sigma} \Big[t(\mathbf{T_i} + \mathbf{r}_{\mathbf{x}_{a_l}}, \mathbf{T_j} + \mathbf{r}_{\mathbf{y}_{a'_l}})\, c^\dagger_\sigma(\mathbf{i}, \mathbf{x}_{a_l})\, c_\sigma(\mathbf{j}, \mathbf{y}_{a'_l}) + \text{h.c.} \Big] \\ & + \sum_{\langle \mathbf{ix},\mathbf{jy}\rangle, a, a', \sigma} \Big[t(\mathbf{T_i} + \mathbf{r}_{\mathbf{x}_{a_1}}, \mathbf{T_j} + \mathbf{r}_{\mathbf{y}_{a'_2}})\, c^\dagger_\sigma(\mathbf{i}, \mathbf{x}_{a_1})\, c_\sigma(\mathbf{j}, \mathbf{y}_{a'_2}) + \text{h.c.} \Big],\end{aligned} \tag{13}$$

where $\mathbf{T_j} = i\mathbf{T}_1 + j\mathbf{T}_2$, and $c^\dagger_\sigma(\mathbf{i}, \mathbf{x}_{a_l})$ is the creation operator of an electron with the spin σ on the sublattice a_l $(= A_l, B_l)$ in the supercell $\mathbf{i}$ in the position $\mathbf{x}$ on layer l.

Note that the Hamiltonian is invariant with respect to translation by $\mathbf{T}_{1,2}$, so we can perform the Fourier transform

$$\varphi^{(l)}_{\mathbf{k},a,\sigma}(\mathbf{x}) = \frac{1}{\sqrt{N_s}} \sum_{\mathbf{j}} e^{i\mathbf{k}\cdot\mathbf{T_j}}\, c_\sigma(\mathbf{i}, \mathbf{x}_{a_l}), \tag{14}$$

where N_s is the number of the supercells. Note that

$$t(\mathbf{T_i} + \mathbf{r_x}, \mathbf{T_j} + \mathbf{r_y}) = t(\mathbf{T_i} - \mathbf{T_j} + \mathbf{r_x} - \mathbf{r_y}), \tag{15}$$

so that we have the Bloch Hamiltonian

$$\mathcal{H}_\mathbf{k}(\mathbf{x}, \mathbf{y}) = \sum_{\mathbf{i}} \mathcal{H}(\mathbf{x}, \mathbf{y} + \mathbf{T_i})\, e^{i\mathbf{k}\cdot\mathbf{T_i}}. \tag{16}$$

Introducing the N-component operator

$$\Phi_{\mathbf{k}\sigma}(\mathbf{x}) = \Big[\varphi^{(1)}_{\mathbf{k},A,\sigma}, \varphi^{(1)}_{\mathbf{k},B,\sigma}, \varphi^{(2)}_{\mathbf{k},A,\sigma}, \varphi^{(2)}_{\mathbf{k},B,\sigma} \Big]^T, \tag{17}$$

we have the Hamiltonian in the form $H = 1/N_s \sum_{\mathbf{k}\sigma} \sum_{\mathbf{x},\mathbf{y}} \Phi^\dagger_{\mathbf{k}\sigma}(\mathbf{x})\, H_\mathbf{k}(\mathbf{x}, \mathbf{y})\, \Phi_{\mathbf{k}\sigma}(\mathbf{y})$, with the matrix elements indicated in Eq. (5) of the main text.

The energy spectrum $\varepsilon_{n\mathbf{k}}$ and the corresponding Bloch state $|\hat{\psi}_{n,\mathbf{k},\sigma}\rangle$ with n band indices can be obtained by diagonalizing the above Hamiltonian matrix:

$$\sum_{\mathbf{y}} \mathcal{H}_\mathbf{k}(\mathbf{x}, \mathbf{y})\, \langle \mathbf{y} | \hat{\psi}_{n,\mathbf{k},\sigma}\rangle = \varepsilon_{n\mathbf{k}}\, \langle \mathbf{x} | \hat{\psi}_{n,\mathbf{k},\sigma}\rangle. \tag{18}$$

Note that the Bloch wavefunctions $\hat{\psi}_{n,\mathbf{k},\sigma}(\mathbf{r_x}) = \langle \mathbf{x} | \hat{\psi}_{n,\mathbf{k},\sigma}\rangle$ satisfy

$$\hat{\psi}_{n,\mathbf{k},\sigma}(\mathbf{r_x} + \mathbf{T_i}) = e^{i\mathbf{k}\cdot\mathbf{T_i}}\, \hat{\psi}_{n,\mathbf{k},\sigma}(\mathbf{r_x}), \tag{19}$$

and the orthogonality

$$\langle \hat{\psi}_{n,\mathbf{k},\sigma} | \hat{\psi}_{n',\mathbf{p},\sigma}\rangle = \sum_{\mathbf{ix}} \hat{\psi}^\dagger_{n,\mathbf{k},\sigma}(\mathbf{r_x} + \mathbf{T_i})\, \hat{\psi}_{n',\mathbf{k},\sigma}(\mathbf{r_x} + \mathbf{T_i}) = N_s\, \delta_{\mathbf{k},\mathbf{p}} \delta_{n,n'}. \tag{20}$$

Since the periodicity of the Bloch wavefunctions, we will use $\mathbf{r} \equiv \mathbf{r_x} + \mathbf{T_j}$ for the atomic positions in the entire lattice. In our calculation, the momentum mesh points (k_1, k_2) is generated by the reciprocal superlattice vectors $\mathbf{G}_1$ and $\mathbf{G}_2$ by $\mathbf{k} = k_1\mathbf{G}_1 + k_2\mathbf{G}_2$ using periodic boundary condition, and we used 300×300 grid points including Γ, K_1, and K_2 in the mini Brillouin zone.

WANNIER FUNCTIONS

The Wannier function centered at $\mathbf{R}$ associated with an energy band n is

$$|\mathbf{R}n\rangle = \frac{1}{N}\sum_{\mathbf{k}} e^{-i\mathbf{k}\cdot\mathbf{R}}|\hat{\psi}_{n\mathbf{k}}\rangle. \tag{21}$$

However, the Wannier functions are not unique, so given one set of of Bloch orbitals, another equally good set is obtained from

$$|\hat{u}_{\mu\mathbf{k}}\rangle \to \sum_{n} U_{n\mu}(\mathbf{k})\,|\hat{u}_{n\mathbf{k}}\rangle, \tag{22}$$

where $|u_{n\mathbf{k}}\rangle = e^{-i\mathbf{k}\cdot\mathbf{r}}|\psi_{n\mathbf{k}}\rangle$ is the periodic part of the Bloch function, and $U_{n\mu}(\mathbf{k})$ is a unitary matrix that mixes the bands at $\mathbf{k}$:

$$\sum_{n} U^*_{n\mu}(\mathbf{k})\,U_{n\mu}(\mathbf{k}) = \delta_{\mu\nu}. \tag{23}$$

The transformation does not preserve the individual Wannier centers, but does preserve the the sum of the the Wannier centers, modulo a lattice vector $\mathbf{T}$. Therefore, the general Wannier function can be written as

$$|\mathbf{R}\mu\rangle = \frac{1}{N}\sum_{\mathbf{k},n} e^{-i\mathbf{k}\cdot\mathbf{R}}U_{n\mu}(\mathbf{k})\,|\hat{\psi}_{n\mathbf{k}}\rangle, \tag{24}$$

or, we can define $W_\mu(\mathbf{r}-\mathbf{R})$ as a localized function at $\mathbf{R}$:

$$\hat{W}_\mu(\mathbf{r}-\mathbf{R}) = \langle\mathbf{r}|\mathbf{R}\mu\rangle = \frac{1}{N}\sum_{\mathbf{k},n} e^{-i\mathbf{k}\cdot\mathbf{R}}U_{n\mu}(\mathbf{k})\,\hat{\psi}_{n\mathbf{k}}(\mathbf{r}). \tag{25}$$

Note that the Wannier function translated by $\mathbf{T_i}$ is orthogonal: Since

$$\begin{aligned}\hat{W}_\mu(\mathbf{r}-\mathbf{R}+\mathbf{T_i}) &= \langle\mathbf{r}+\mathbf{T_i}|\mathbf{R}\mu\rangle = \langle\mathbf{r}|\mathbf{R}-\mathbf{T_i},\mu\rangle \\ &= \frac{1}{N}\sum_{\mathbf{k},n} e^{-i\mathbf{k}\cdot(\mathbf{R}-\mathbf{T_i})}U_{n\mu}(\mathbf{k})\,\hat{\psi}_{n\mathbf{k}}(\mathbf{r}),\end{aligned} \tag{26}$$

we have

$$\begin{aligned}\langle\mathbf{R}\mu|\mathbf{R}-\mathbf{T_i},\nu\rangle &= \frac{1}{N^2}\sum_{\mathbf{k},\mathbf{p},n,n'} U^*_{n\mu}(\mathbf{k})U_{n'\nu}(\mathbf{p})\,e^{i\mathbf{p}\cdot\mathbf{T_i}}\,\langle\hat{\psi}_{n\mathbf{k}}|\hat{\psi}_{n',\mathbf{p}}\rangle \\ &= \frac{1}{N}\sum_{\mathbf{k},n} U^*_{n\mu}(\mathbf{k})U_{n\nu}(\mathbf{k})\,e^{i\mathbf{k}\cdot\mathbf{T_i}} = \frac{1}{N}\sum_{\mathbf{k}}\delta_{\mu\nu}\,e^{i\mathbf{k}\cdot\mathbf{T_i}} \\ &= \delta_{\mu\nu}\,\delta_{\mathbf{T_i},\mathbf{0}}.\end{aligned}$$

As a measure of the delocalization or spread of the Wannier functions, $\Omega[U(\mathbf{k})] = \sum_\mu \left[\langle r^2\rangle_\mu - \langle r_\mu\rangle^2\right]$ with $\langle r_\mu\rangle = \langle\mathbf{0}\mu|r|\mathbf{0}\mu\rangle$ and $\langle r^2\rangle_\mu = \langle\mathbf{0}\mu|r^2|\mathbf{0}\mu\rangle$, the maximally localized Wannier functions can be obtained by minimizing Ω with respect to $U_{n\mu}(\mathbf{k})$ [8].

SITE-SYMMETRY GROUP AND SYMMETRY-ADAPTED WANNIER FUNCTIONS

Specifying a set of sites $\{\mathbf{R}_1,\mathbf{R}_2,\cdots\}$, where the Wannier functions will be centered, the site-symmetry group of a given $\mathbf{R}_1$, denoted by $G_{\rm site}$, is a subgroup of the full symmetry group of the lattice, G whose elements leave $\mathbf{R}_1$ unchanged, so $g_{\rm site} = (R_s|\mathbf{T}_s) \in G_{\rm site}$ satisfy

$$g_{\rm site}\,\mathbf{R}_1 = (R_s|\mathbf{T}_s)\mathbf{R}_1 = R_s\mathbf{R}_1 + \mathbf{T}_s = \mathbf{R}_1, \tag{27}$$

where R_s, $\mathbf{T}_s$ are the rotation and the translation part of the symmetry operation. The full symmetry group G can be decomposed into left cosets of the subgroup $G_{\rm site}$ as

$$G = \sum_{j,n} g_{jn} G_{\rm site}, \quad g_{jn} = (R_j|\mathbf{T}_j + \mathbf{T}_n). \tag{28}$$

Here, g_{j0} ($\mathbf{T}_0 = \mathbf{0}$) is one of the symmetry operations that maps $\mathbf{R}_1$ to its symmetry-equivalent point $\mathbf{R}_j$ as

$$\mathbf{R}_j = g_{j0}\mathbf{R}_1 = R_j\mathbf{R}_1 + \mathbf{T}_j. \tag{29}$$

Since $j = 1$ corresponds to the original point $\mathbf{R}_1$, $g_{10} = (E|\mathbf{0})$, where E denotes the identity operation.

From the site-symmetry group for a given $\mathbf{R}_1$, the site-symmetry adapted Wannier functions centered at $\mathbf{R}_1$ are defined as the basis functions of the irreducible representations of the site-symmetry group $G_{\rm site}$. These Wannier functions are represented as

$$\hat{W}_\alpha(\mathbf{r}_j) \equiv \hat{W}_\alpha(\mathbf{r} - \mathbf{R}_j), \tag{30}$$

where $\alpha = 1, 2, \cdots, n_\alpha$ denote the component of the basis functions with n_α the dimension of the irreducible representation. The Wannier functions transform as

$$\hat{g}_{\rm site}\hat{W}_\alpha(\mathbf{r}) \;=\; \hat{W}_\alpha(g_{\rm site}^{-1}\mathbf{r} - \mathbf{R}_1) = \sum_{\alpha'=1}^{n_\alpha} d_{\alpha'\alpha}(R_s)\,\hat{W}_{\alpha'}(\mathbf{r}_1) \tag{31}$$

From $\hat{W}_{\alpha 1}(\mathbf{r})$, we can generate Wannier functions centered at $\mathbf{R}_j$ as

$$\hat{W}_\alpha(\mathbf{r}_j) = \hat{g}_{j0}\,\hat{W}_\alpha(\mathbf{r}_1). \tag{32}$$

In our model, $\hat{g}_{\rm site} = \hat{C}_3$ and $\mathbf{R}_1$ is a site BA, leading to $\hat{W}_1(\mathbf{r}_1) = \hat{W}_+(\mathbf{r}_1) = \hat{W}_+(\mathbf{r} - \mathbf{R}_1)$ and $\hat{W}_2(\mathbf{r}_1) = W_-(\mathbf{r}_1) = W_-(\mathbf{r} - \mathbf{R}_1)$ with

$$d_{\alpha'\alpha} = \begin{pmatrix} \epsilon & 0 \\ 0 & \epsilon^* \end{pmatrix}, \quad \alpha', \alpha = 1, 2, \quad \epsilon = \exp(2\pi i/3). \tag{33}$$

For $\mathbf{R}_2$ a site AB, we have $\hat{W}_1(\mathbf{r}_2) = \hat{W}_-(\mathbf{r}_2) = \hat{W}_-(\mathbf{r} - \mathbf{R}_2)$ and $\hat{W}_2(\mathbf{r}_2) = \hat{W}_+(\mathbf{r}_2) = \hat{W}_+(\mathbf{r} - \mathbf{R}_2)$ with $R_2 = C'_{2y}$.

From these symmetry-adapted Wannier functions $W_{\alpha j}(\mathbf{r})$, one can construct the Bloch functions $\Psi_{\mathbf{k},\alpha j}(\mathbf{r})$ as

$$\hat{\psi}_{\mathbf{k},\alpha}(\mathbf{r}_j) \;=\; \sum_n e^{i\mathbf{k}\cdot\mathbf{T}_n}\hat{W}_\alpha(\mathbf{r}_j - \mathbf{T}_n) \tag{34}$$

$$\hat{W}_\alpha(\mathbf{r}_j - \mathbf{T}_n) \;=\; \frac{1}{N_s}\sum_{\mathbf{k}} e^{-i\mathbf{k}\cdot\mathbf{T}_n}\hat{\psi}_{\mathbf{k},\alpha}(\mathbf{r}_j). \tag{35}$$

These site-symmetry adapted wannier functions and the Bloch functions transform as

$$\hat{g}\hat{W}_\alpha(\mathbf{r}_j - \mathbf{T}_n) \;=\; \sum_{\alpha'=1}^{n_\alpha} d_{\alpha'\alpha}(R_{j'}^{-1}\,R\,R_j)\,W_{\alpha' j'}(\mathbf{r} - \mathbf{T}_{j'j} - R\mathbf{T}_n) \tag{36}$$

$$\hat{g}\Psi_{\mathbf{k},\alpha}(\mathbf{r}_j) \;=\; \sum_{\alpha'=1}^{n_\alpha} d_{\alpha'\alpha}(R_{j'}^{-1}\,R\,R_j)\,\psi_{R\mathbf{k},\alpha' j'}(\mathbf{r})\,e^{-iR\mathbf{k}\cdot\mathbf{T}_{j'j}}, \tag{37}$$

where $R = R_{j'}\,R_s\,R_j^{-1}$ and $\mathbf{T}_{j'j} = g\mathbf{R}_j - \mathbf{R}_{j'}$. The index j' is determined by g and g_j to maintain $\mathbf{T}_{j'j}$ being lattice vectors. Then the irreducible representation of G is given by

$$D_{\alpha' j',\alpha j}(g,\mathbf{k}) = e^{-iR\mathbf{k}\cdot\mathbf{T}_{j'j}}\,d^{(\beta)}_{\alpha'\alpha}(R_{j'}^{-1}\,R\,R_j). \tag{38}$$

The unitary matrix (22) for the maximally localized Wannier functions with the site-symmetry adapted can be obtained by solving

$$U_{n\mu}(R\mathbf{k}) = \tilde{d}_{n,n'}(g,\mathbf{k})\,U_{n',\mu'}(\mathbf{k})\,D^\dagger_{\mu',\mu}(g,\mathbf{k}), \tag{39}$$

where

$$\tilde{d}_{n,n'}(g,\mathbf{k}) = \int d\mathbf{r}\, \hat{\psi}^{\dagger}_{n,R\mathbf{k}}(\mathbf{r})\hat{\psi}_{n',\mathbf{k}}(g^{-1}\mathbf{r}) \tag{40}$$

with $\hat{\psi}_{n\mathbf{k}}(\mathbf{r})$ the eigenfunctions of the Bloch Hamiltonian. Here, we used the notation, $\mu = \{\alpha j\}$. With these $D_{\alpha' j',\alpha j}(g,\mathbf{k})$, $d_{\alpha'\alpha}(R_s)$, and $\tilde{d}_{n',n}(g,\mathbf{k})$ as inputs for the Wannier90 package [10], we can find the site-symmetry adapted Bloch wavefunction, Eq. (34), as

$$\hat{\Psi}_{\mathbf{k},\alpha}(\mathbf{r}_j) = \sum_n U_{n,\alpha j}(\mathbf{k})\, \hat{\psi}_{n\mathbf{k}}(\mathbf{r}), \tag{41}$$

leading to the site-symmetry enforced Wannier functions, Eq. (35).

TIGHT-BINDING HAMILTONIAN

Hopping amplitude

The most general tight-binding Hamiltonian is of the form

$$\mathcal{H}_0 = \sum_{\alpha\beta=\pm} \sum_{j,j'=BA,AB} t_{\alpha\beta}(\mathbf{R}_j - \mathbf{R}_{j'})\, d^{\dagger}_{\alpha}(\mathbf{R}_j)\, d_{\beta}(\mathbf{R}_{j'}), \tag{42}$$

where the creation operator $d_\alpha(\mathbf{R}_j)$ is associated with the Wannier functions

$$|\mathbf{R}_j, \alpha\rangle = d^{\dagger}_{\alpha}(\mathbf{R}_j)|0\rangle. \tag{43}$$

Then the hopping amplitude $t_{\alpha\beta}(\mathbf{R}_{jj'})$ is given by

$$\begin{aligned} t_{\alpha\beta}(\mathbf{R}_{jj'}) &= \langle \mathbf{R}_j, \alpha|\, H\, |\mathbf{R}_{j'}, \beta\rangle \\ &= \int d\mathbf{r} d\mathbf{r}' \hat{W}^{\dagger}_{\alpha}(\mathbf{r}_j)\, H(\mathbf{r},\mathbf{r}')\, \hat{W}_{\beta}(\mathbf{r}'_{j'}) \\ &= \frac{1}{N_s}\sum_{\mathbf{k},\alpha'} U^{*}_{\alpha'\alpha}(\mathbf{k}) U_{\alpha'\beta}(\mathbf{k})\, e^{-i\mathbf{k}\cdot\mathbf{T}_{jj'}} \int d\mathbf{r} d\mathbf{r}' \hat{\psi}^{\dagger}_{\alpha'\mathbf{k}}(\mathbf{r}) H_{\mathbf{k}}(\mathbf{r},\mathbf{r}')\, \hat{\psi}_{\alpha'\mathbf{k}}(\mathbf{r}') \\ &= \frac{1}{N_s}\sum_{\mathbf{k},\alpha'} U^{*}_{\alpha'\alpha}(\mathbf{k}) U_{\alpha'\beta}(\mathbf{k})\, \varepsilon_{\alpha'}(\mathbf{k})\, e^{-i\mathbf{k}\cdot\mathbf{T}_{jj'}}, \end{aligned} \tag{44}$$

where $\mathbf{T}_{jj'} = \mathbf{T}_{j'} - \mathbf{T}_j$, with $\mathbf{T}_j$ the lattice vector of the cell enclosing $\mathbf{R}_j$.

Interaction Hamiltonian

The exchange interaction follows from the Coulomb interaction

$$\mathcal{H}_C = \frac{1}{2}\int \mathrm{d}\mathbf{r}\mathrm{d}\mathbf{r}' \rho(\mathbf{r}) \frac{e^2}{|\mathbf{r}-\mathbf{r}'|}\rho(\mathbf{r}'), \tag{45}$$

where $\rho(\mathbf{r}) = \sum_\sigma \Psi^{\dagger}_{\sigma}(\mathbf{r})\cdot\Psi_\sigma(\mathbf{r})$ are density operators written in terms of field operators

$$\Psi_\sigma(\mathbf{r}) = \sum_{\alpha,j} W(\mathbf{r}-\mathbf{R}_j) d_{j,\alpha,\sigma}.$$

The most general exchange term between sites i, j that follows from (45) has the form

$$H_J = \sum_{i\neq j}\sum_{\alpha\beta\alpha'\beta'}\sum_{\sigma,\sigma'} J_{ij,\alpha\alpha'\beta\beta'}\, d^{\dagger}_{i,\alpha,\sigma} d^{\dagger}_{j,\beta,\sigma'} d_{i\beta',\sigma'} d_{j,\alpha',\sigma},$$

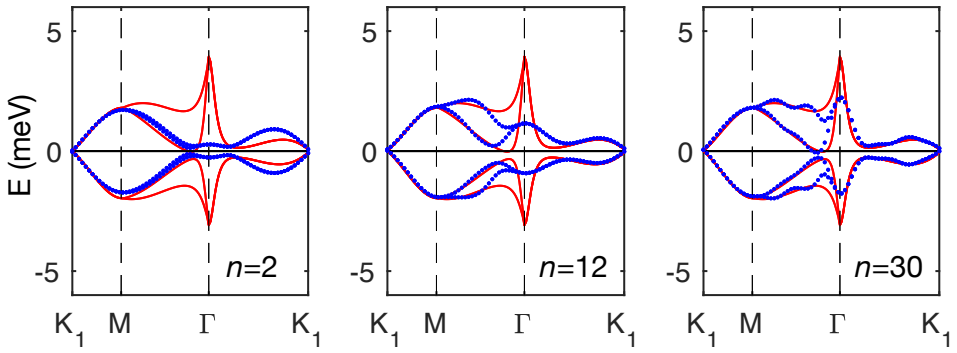


FIG. 1: Band structure constructed by the Wannier orbitals. The red solid lines represents the microscopic Bloch bands and the blue dots represent the Bloch bands constructed using the Wannier orbitals of the n nearest-neighbors. $n = 2, 12$, and 30 correspond to the ranges $L = |\mathbf{T}|, 3|\mathbf{T}|$, and $5|\mathbf{T}|$, respectively. As L increases, the values of Γ point become closer to the microscopic Bloch bands.

where

$$J_{ij,\alpha\alpha'\beta\beta'} = \frac{1}{2}\int \mathrm{d}^2r\mathrm{d}^2r' \sum_{\alpha\alpha'\beta\beta'} W^\dagger_\alpha(\mathbf{r}-\mathbf{R}_i)\cdot W_{\alpha'}(\mathbf{r}-\mathbf{R}_j)\frac{e^2}{|\mathbf{r}-\mathbf{r}'|}W^\dagger_\beta(\mathbf{r}'-\mathbf{R}_j)\cdot W_{\beta'}(\mathbf{r}-\mathbf{R}_i) \tag{46}$$

is the exchange coupling. We find numerically that only the $J_{ij,\alpha\alpha\beta\beta} \equiv J_{ij,\alpha\beta}$ combination is non-zero. The exchange interaction has the form

$$\mathcal{H}_J = \sum_{i\neq j}\sum_{\alpha\beta}\sum_{\sigma,\sigma'} J_{ij,\alpha\beta}\, d^\dagger_{i,\alpha,\sigma} d^\dagger_{j,\beta,\sigma'} d_{i\beta,\sigma'} d_{j,\alpha,\sigma}. \tag{47}$$

Now mapping the d operators into spin and pseudo-spin operators [9, 11],

$$\begin{aligned}
d^\dagger_{\alpha\sigma}d_{\alpha\sigma} &\rightarrow \left(\frac{1}{2}+\alpha\tau^z\right)\left(\frac{1}{2}+\sigma S^z\right)\\
d^\dagger_{\alpha\sigma}d_{\alpha-\sigma} &\rightarrow \left(\frac{1}{2}+\alpha\tau^z\right)S^\sigma\\
d^\dagger_{\alpha\sigma}d_{-\alpha\sigma} &\rightarrow \tau^\alpha\left(\frac{1}{2}+\sigma S^z\right)\\
d^\dagger_{\alpha\sigma}d_{-\alpha-\sigma} &\rightarrow \tau^\alpha S^\sigma
\end{aligned}$$

with $\alpha = \pm$ and $\sigma = \pm$ and $\tau^\alpha = \tau^x + i\alpha\tau^y$, $S^\sigma = S^x + i\sigma S^y$, (47) can be cast into the form

$$\mathcal{H}_e = -\sum_{\sigma\sigma'}\sum_{\alpha\beta} J_{ij,\alpha\alpha}\left(\frac{1}{2}+2\tau^z_i\tau^z_j - 2\tau^x_i\tau^x_j - 2\tau^y_i\tau^y_j\right)\left(\frac{1}{2}+2\mathbf{S}_i\cdot\mathbf{S}_j\right). \tag{48}$$

NUMERICAL DETAILS

Our calculations are carried out with the tight-binding Bloch Hamiltonian of the microscopic twisted graphene bilayer. The maximally localized Wannier orbitals were found with the Wannier90 package. The momentum space $\mathbf{k}$ mesh points were generated by the reciprocal supercell lattice vectors $\mathbf{G}_1$ and $\mathbf{G}_2$ by $\mathbf{k} = k_1\mathbf{G}_1 + k_2\mathbf{G}_2$ with 300×300 grid points using periodic boundary conditions. This way, the Brillouin zone includes Γ, K_1, and K_2 high symmetric points. We modified the code in the package for the Brillouin zone to include all the $\mathbf{k}$ points and the corresponding $-\mathbf{k}$ points (modulo a reciprocal lattice vectors), reflecting the time-reversal conjugates of the Bloch wavefunctions.

In order to implement the Wannier90 package to find the maximally localized Wannier functions, we provided initial wavefunctions using the Bloch wavefunctions at the Γ point as input functions. At that point, the Bloch wavefunctions

1st nearest-neighbor hoppings

(m,n)	$(0,0)$	$(0,-1)$	$(-1,0)$
$t_{++}^{(BA,AB)}(\boldsymbol{\delta})$	$0.004+0.385i$	$0.004+0.385i$	$0.004+0.385i$
$t_{--}^{(BA,AB)}(\boldsymbol{\delta})$	$0.121-0.363i$	$0.121-0.363i$	$0.121-0.363i$

2nd nearest-neighbor hoppings

(m,n)	$(0,1)$	$(0,-1)$	$(-1,0)$	$(1,0)$	$(-1,1)$	$(1,-1)$
$t_{++}^{(BA,BA)}(\boldsymbol{\delta})$	$0.004+0.002i$	$0.004-0.002i$	$-0.000+0.000i$	$-0.000-0.000i$	$0.004-0.002i$	$0.004+0.002i$
$t_{++}^{(AB,AB)}(\boldsymbol{\delta})$	$-0.001-0.002i$	$-0.001+0.002i$	$0.002-0.000i$	$0.002+0.000i$	$-0.002+0.002i$	$-0.002-0.002i$
$t_{--}^{(BA,BA)}(\boldsymbol{\delta})$	$0.002-0.007i$	$0.002+0.007i$	$-0.002-0.009i$	$-0.002+0.009i$	$0.002+0.008i$	$0.002-0.008i$
$t_{--}^{(AB,AB)}(\boldsymbol{\delta})$	$0.000+0.007i$	$0.000-0.007i$	$0.004+0.009i$	$0.004-0.009i$	$0.000-0.008i$	$0.000+0.008i$

3rd nearest-neighbor hoppings

(m,n)	$(-1,-1)$	$(-1,1)$	$(1,-1)$
$t_{++}^{(BA,AB)}$	$0.065-0.442i$	$0.065-0.442i$	$0.065-0.442i$
$t_{--}^{(BA,AB)}$	$-0.071+0.441i$	$-0.071+0.441i$	$-0.071+0.441i$

4th nearest-neighbor hoppings

(m,n)	$(0,1)$	$(0,-2)$	$(1,0)$	$(1,-2)$	$(-2,0)$	$(-2,1)$
$t_{++}^{(BA,BA)}(\boldsymbol{\delta})$	$-0.040-0.157i$	$-0.039-0.157i$	$-0.039-0.158i$	$-0.040-0.157i$	$-0.040-0.157i$	$-0.040-0.157i$
$t_{++}^{(AB,AB)}(\boldsymbol{\delta})$	$-0.040+0.157i$	$-0.039+0.157i$	$-0.040+0.158i$	$-0.040+0.157i$	$-0.040+0.157i$	$-0.040+0.157i$
$t_{--}^{(BA,BA)}(\boldsymbol{\delta})$	$0.009+0.163i$	$0.008+0.163i$	$0.008+0.163i$	$0.009+0.163i$	$0.009+0.163i$	$0.008+0.163i$
$t_{--}^{(AB,AB)}(\boldsymbol{\delta})$	$0.009-0.163i$	$0.008-0.163i$	$0.008-0.163i$	$0.009-0.163i$	$0.009-0.163i$	$0.008-0.163i$

5th nearest-neighbor hoppings

(m,n)	$(1,1)$	$(-1,-1)$	$(-1,2)$	$(1,-2)$	$(-2,1)$	$(2,-1)$
$t_{++}^{(BA,BA)}(\boldsymbol{\delta})$	$0.011+0.081i$	$0.011-0.081i$	$0.013-0.084i$	$0.013+0.084i$	$0.008+0.084i$	$0.008-0.084i$
$t_{++}^{(AB,AB)}(\boldsymbol{\delta})$	$0.009+0.085i$	$0.009-0.085i$	$0.007-0.082i$	$0.007+0.082i$	$0.012+0.082i$	$0.012-0.082i$
$t_{--}^{(BA,BA)}(\boldsymbol{\delta})$	$0.011-0.084i$	$0.011+0.084i$	$0.014+0.083i$	$0.014-0.083i$	$0.006-0.081i$	$0.006+0.081i$
$t_{--}^{(AB,AB)}(\boldsymbol{\delta})$	$0.009-0.082i$	$0.009+0.082i$	$0.007+0.083i$	$0.007-0.083i$	$0.014-0.085i$	$0.014+0.085i$

6th nearest-neighbor hoppings

(m,n)	$(0,2)$	$(0,-2)$	$(-2,0)$	$(2,0)$	$(-2,2)$	$(2,-2)$
$t_{++}^{(BA,BA)}(\boldsymbol{\delta})$	$0.005+0.007i$	$0.005-0.007i$	$-0.005+0.001i$	$-0.005-0.001i$	$-0.000-0.001i$	$-0.000+0.001i$
$t_{++}^{(AB,AB)}(\boldsymbol{\delta})$	$-0.003-0.007i$	$-0.003+0.007i$	$0.006-0.001i$	$0.006+0.001i$	$0.002+0.001i$	$0.002-0.001i$
$t_{--}^{(BA,BA)}(\boldsymbol{\delta})$	$0.006-0.003i$	$0.006+0.003i$	$-0.006-0.012i$	$-0.006+0.012i$	$0.001+0.010i$	$0.001-0.010i$
$t_{--}^{(AB,AB)}(\boldsymbol{\delta})$	$-0.004+0.003i$	$-0.004-0.003i$	$0.008+0.012i$	$0.008-0.012i$	$0.001-0.010i$	$0.001+0.010i$

TABLE I: The nearest-neighbor vectors $\boldsymbol{\delta}=m\mathbf{T}_1+n\mathbf{T}_2$, where $\mathbf{T}_j$ are the superlattice primitive vectors. The superscript of $t_{\alpha\beta}^{(X,Y)}(\boldsymbol{\delta})$ indicates the hopping from the sublattice $|X,\alpha\rangle$ to $|Y,\beta\rangle$ with $X,Y=BA,AB$. In the momentum space, the Bloch Hamiltonian can be expressed by $t_{\alpha\beta}^{(X,Y)}(\mathbf{k})=\sum_{\boldsymbol{\delta}}t_{\alpha\beta}^{(X,Y)}(\boldsymbol{\delta})\exp(i\mathbf{k}\cdot\boldsymbol{\delta})$.

satisfy

$$\hat{C}_3\,\hat{\psi}_{1(3),\Gamma}(\mathbf{r})=\epsilon\hat{\psi}_{1(3),\Gamma}(\mathbf{r})$$

and

$$\hat{C}_3\,\hat{\psi}_{2(4),\Gamma}(\mathbf{r})=\epsilon^*\hat{\psi}_{2(4),\Gamma}(\mathbf{r}),$$

with $\epsilon=\exp^{i2\pi/3}$. The Bloch wavefunctions also satisfy $\hat{C}'_{2y}\,\psi_{1(2),\Gamma}(\mathbf{r})=\hat{\psi}_{3(4),\Gamma}(\mathbf{r})$ with $\psi_{3(4),\Gamma}(\mathbf{r})$ being the C_3 eigenstates with $\epsilon^*(\epsilon)$, respectively. The four Wannier state spinors were derived from the input wavefunctions

$$\hat{W}_1^{(0)}(\mathbf{r})=[\psi_{1,\Gamma}(\mathbf{r}_{A_1}),\psi_{3,\Gamma}(\mathbf{r}_{B_1}),\psi_{3,\Gamma}(\mathbf{r}_{A_2}),\psi_{1,\Gamma}(\mathbf{r}_{B_2})]^T,$$

$$\hat{W}_4^{(0)}(\mathbf{r}) = [\psi_{3,\Gamma}(\mathbf{r}_{A_1}), \psi_{1,\Gamma}(\mathbf{r}_{B_1}), \psi_{1,\Gamma}(\mathbf{r}_{A_2}), \psi_{3,\Gamma}(\mathbf{r}_{B_2})]^T,$$

$$\hat{W}_2^{(0)}(\mathbf{r}) = [\psi_{4,\Gamma}(\mathbf{r}_{A_1}), \psi_{2,\Gamma}(\mathbf{r}_{B_1}), \psi_{2,\Gamma}(\mathbf{r}_{A_2}), \psi_{4,\Gamma}(\mathbf{r}_{B_2})]^T,$$

and

$$\hat{W}_3^{(0)}(\mathbf{r}) = [\psi_{2,\Gamma}(\mathbf{r}_{A_1}), \psi_{4,\Gamma}(\mathbf{r}_{B_1}), \psi_{4,\Gamma}(\mathbf{r}_{A_2}), \psi_{2,\Gamma}(\mathbf{r}_{B_2})]^T.$$

The first two input functions are eigenstates of the C_3 operator with eigenvalues ϵ, while the other two with eigenvalues ϵ^*.

To obtain the maximally localized Wannier functions $\hat{W}_{1(2)}(\mathbf{r})$ at BA site and $\hat{W}_{3(4)}(\mathbf{r})$ at AB site, the initial wavefunctions are multiplied by Gaussian functions centered at those points. The resulting Wannier functions reflect the D_3 symmetry of the lattice, $C_3\,\hat{W}_{1(4)}(\mathbf{r}) = \epsilon\hat{W}_{1(4)}(\mathbf{r})$ and $C_3\,\hat{W}_{2(3)}(\mathbf{r}) = \epsilon^*\hat{W}_{2(3)}(\mathbf{r})$, and $C'_{2y}\,\hat{W}_{1(2)}(\mathbf{r}) = \hat{W}_{3(4)}(\mathbf{r})$, while $W^*_{1(4)}(\mathbf{r}) = W_{2(3)}(\mathbf{r})$. Therefore, we label the four degenerate Wannier function spinors as $\hat{W}_{1(3)}(\mathbf{r}) = \hat{W}_+(\mathbf{r}-\mathbf{R}_1)$ and $\hat{W}_{2(4)}(\mathbf{r}) = \hat{W}_-(\mathbf{r}-\mathbf{R}_2)]$, where $\mathbf{R}_{1(2)}$ represents a $BA(AB)$ site.

[1] S. Shallcross, S. Sharma, and O. Pankratov, Phys. Rev. B **87**, 245403 (2013).
[2] S. Shallcross, S. Sharma, E. Kandelaki, and O. Pankratov, Phys. Rev. B **81**, 1 (2010).
[3] E. J. Mele, J. Phys. D **45**, 154004 (2012).
[4] J. M. B. Lopes dos Santos, N. M. R. Peres, and A. H. Castro Neto, Phys. Rev. Lett. **99**, 256802 (2007).
[5] J. M. B. Lopes dos Santos, N. M. R. Peres, and A. H. Castro Neto, Phys. Rev. B **86**, 155449 (2012).
[6] M. S. Tang, C. Z. Wang, C. T. Chan, and K. M. Ho, Phys. Rev. B **53**, 979, (1996).
[7] I. Brihuega, P. Mallet, H. Gonzlez-Herrero, G. Trambly de Laissardire, M. M. Ugeda, L. Magaud, J. M. Gmez-Rodrguez, F. Yndurin, and J.-Y. Veuillen Phys. Rev. Lett. **109**, 196802 (2012).
[8] Nicola Marzari and David Vanderbilt, Phys. Rev. B **56**, 12847 (1997).
[9] Bruno Uchoa, Valeri N. Kotov, and M. Kindermann, Phys. Rev. B **91**, 121412(R) (2015).
[10] A. A. Mostofi, J. R. Yates, G. Pizzi, Y.-S. Lee, I. Souza, D. Vanderbilt, and N. Marzari, *WANNIER90: A Tool for Obtaining Maximally-Localised Wannier Functions*, Comput. Phys. Commun. **185**, 2309 (2014).
[11] K. I. Kugel and D. I. Khomskii, Sov. Phys. Uspekhi **25**, 231 (1982).